Neurobiology of Aging 69 (2018) 199–208

Contents lists available at ScienceDirect

Neurobiology of Aging

journal homepage: www.elsevier.com/locate/neuaging

[^{18}F]FMPEP-d_2 PET imaging shows age- and genotype-dependent impairments in the availability of cannabinoid receptor 1 in a mouse model of Alzheimer's disease

Jatta S. Takkinen [a,b,c,*], Francisco R. López-Picón [a,b], Anna K. Kirjavainen [d], Rea Pihlaja [a,b], Anniina Snellman [a,b], Tamiko Ishizu [a,e], Eliisa Löyttyniemi [f], Olof Solin [d,g,h], Juha O. Rinne [i,j], Merja Haaparanta-Solin [a,b]

[a] MediCity Research Laboratory, University of Turku, Turku, Finland
[b] PET Preclinical Laboratory, Turku PET Centre, University of Turku, Turku, Finland
[c] Doctoral Programme in Clinical Research, University of Turku, Turku, Finland
[d] Radiopharmaceutical Chemistry Laboratory, Turku PET Centre, University of Turku, Turku, Finland
[e] Institute of Biomedicine, University of Turku, Turku, Finland
[f] The Department of Biostatistics, University of Turku, Turku, Finland
[g] Accelerator Laboratory, Turku PET Centre, Åbo Akademi University, Turku, Finland
[h] Department of Chemistry, University of Turku, Turku, Finland
[i] Turku PET Centre, Turku University Hospital, Turku, Finland
[j] Division of Clinical Neurosciences, Turku University Hospital, Turku, Finland

ARTICLE INFO

Article history:
Received 5 December 2017
Received in revised form 9 May 2018
Accepted 11 May 2018
Available online 18 May 2018

Keywords:
Alzheimer's disease
APP/PS1-21
Longitudinal PET imaging
[^{18}F]FMPEP-d_2
Cannabinoid receptor 1

ABSTRACT

Contradictory findings on the role of the type 1 cannabinoid receptor (CB_1R) during the pathogenesis of Alzheimer's disease (AD) have been reported. Here, we evaluated the CB_1R brain profile in an AD mouse model using longitudinal positron emission tomography with an inverse agonist for CB_1R, [^{18}F]FMPEP-d_2. APP/PS1-21 and wild-type (n = 8 in each group) mice were repeatedly imaged between 6 to 15 months of age, accompanied by brain autoradiography, western blot, and CB_1R immunohistochemistry with additional mice. [^{18}F]FMPEP-d_2 positron emission tomography demonstrated lower ($p < 0.05$) binding ratios in the parietotemporal cortex and hippocampus of APP/PS1-21 mice compared with age-matched wild-type mice. Western blot demonstrated no differences between APP/PS1-21 and wild-type mice in the CB_1R abundance, whereas significantly lower ($p < 0.05$) receptor expression was observed in male than female mice. The results provide the first demonstration that [^{18}F]FMPEP-d_2 is a promising imaging tool for AD research in terms of CB_1R availability, but not expression. This finding may further facilitate the development of novel therapeutic approaches based on endocannabinoid regulation.

1. Introduction

Alzheimer's disease (AD) is an age-related neurodegenerative disease characterized by progressive memory loss, cognitive decline, and the accumulation of neuritic β-amyloid plaques and neurofibrillary tangles, associated with elevated neuroinflammation and oxidative stress (Ball, 1976; Glenner et al., 1984). Strong evidence of alterations in the endocannabinoid system (ECS) in the pathogenesis of AD has raised questions about the development of novel therapeutic approaches for AD based on endocannabinoid regulation (Fagan and Campbell, 2015). The ECS is composed of a relatively broad set of receptors, endogenous ligands, and enzymes, which are involved in AD pathogenesis (Karl et al., 2012; Pazos et al., 2004). The type 2 cannabinoid receptor is overexpressed in activated microglia (Benito et al., 2003); however, the role of the type 1 cannabinoid receptor (CB_1R) is unclear because contradictory results from postmortem human AD studies show bipolar changes in receptor regulation or unchanged CB_1R status (Ahmad et al., 2014; Lee et al., 2010; Ramirez et al., 2005; Westlake et al., 1994). Preclinical studies with AD animal models have also yielded contradictory results. Reductions in amyloid plaque load accompanied with impaired learning and memory deficits were demonstrated in CB_1R-deficient APP23 mice (APP23/CB1$^{-/-}$) when compared with APP23 mice, suggesting that CB_1R deficiency worsens learning and memory deficits in AD

* Corresponding author at: University of Turku, Turku PET Centre, Tykistökatu 6 A, FI 20520, Turku, Finland. Tel. +358 2 94503837; fax: +358 2 94505040.
E-mail address: jatta.takkinen@utu.fi (J.S. Takkinen).

https://doi.org/10.1016/j.neurobiolaging.2018.05.013

(Stumm et al., 2013). Significantly decreased CB_1R expression has been observed in the hippocampus (HIPPO) of 10- to 12-month-old $APP_{SWE}/PS1_{\Delta E9}$ mice in association with astrogliosis (Kalifa et al., 2011), whereas increased CB_1R levels have been reported in the cortex of 14-month-old—but not in 7-month-old—$APP_{SWE}/PS1_{\Delta E9}$ mice (Mulder et al., 2011). Moreover, a recent study demonstrated no differences in CB_1R activity in 13- to 14-month-old female $APP_{SWE}/PS1_{\Delta E9}$ mice compared with wild-type (WT) mice (Karkkainen et al., 2012), whereas in 3×Tg-AD mice, thalamic CB_1R activity was up-regulated at 4 months of age, but not in older animals (Manuel et al., 2016).

Consequently, novel CB_1R positron emission tomography (PET) radioligands have been developed to monitor this receptor in CB_1R-related neuronal diseases in vivo. The first CB_1R-related radioligand, (−)-5′-[^{18}F]fluoro-Δ^8-THC, possessed high nonspecific binding, poor blood-brain barrier permeability, and low affinity for the target receptor (Charalambous et al., 1991). It was followed by many more "first-generation" radioligands, such as [^{18}F]AM5144 and [^{11}C]SR149080 (Li et al., 2005; Mathews et al., 2000). The initial "second-generation" radioligand, [^{11}C]OMAR, a rimonabant-like CB_1R antagonist, was reported to have reduced lipophilicity and higher affinity (Horti et al., 2006). Another second-generation radioligand, [^{18}F]MK-9470, is a potent CB_1R inverse agonist with a high affinity, 60-fold selectivity for CB_1R over type 2 cannabinoid receptor, and high specific binding to mammalian brain (Burns et al., 2007).

The newest member of the second-generation CB_1R-PET family is a structural analog for [^{11}C]MePPEP, [^{18}F]FMPEP-d_2, which is extremely lipophilic ($logD_{7.4} \approx 4.2$), yet has >80% specific binding in rhesus monkey brain and is less prone to in vivo defluorination due to its dideuterofluoromethoxy group (Terry, 2009; Tsujikawa et al., 2014). [^{18}F]FMPEP-d_2 has been used in a PET study for imaging brown adipose tissue (Eriksson et al., 2015) and detecting the involvement of the CB_1R system in alcohol dependence (Hirvonen et al., 2013). In AD research, the applicability of this tracer has yet to be examined.

Despite the difficulties of developing suitable PET radioligands for imaging CB_1Rs in vivo, the need is urgent for reliable research tools for studying the role of the ECS in neurological diseases. Therefore, the aim of this study was to evaluate the changes in CB_1Rs and the alterations in [^{18}F]FMPEP-d_2 binding in an aging transgenic (TG) mouse model of AD, APP/PS1-21, using longitudinal [^{18}F]FMPEP-d_2 PET/computed tomography (CT) imaging, ex vivo digital autoradiography, and western blot. Thin-layer chromatography and receptor blocking were used for investigating the metabolism and specific binding of [^{18}F]FMPEP-d_2, respectively. CB_1R abundance in mouse brain was visualized using immunohistochemistry. We hypothesize that [^{18}F]FMPEP-d_2 PET imaging can be used to image the CB_1R-associated pathogenesis in AD, thus paving the way for expanding future drug development strategies.

2. Materials and methods

2.1. [^{18}F]FMPEP-d_2 synthesis

[^{18}F]FMPEP-d_2 ([3*R*,5*R*]-5-((3-([^{18}F]fluoromethoxy-d_2)phenyl)-3-((*R*)-1-phenyl-ethylamino)-1-(4-trifluoromethyl-phenyl)-pyrrolidin-2-one) was synthesized at the Radiopharmaceutical Chemistry Laboratory at the Turku PET Centre. Precursor (3*R*,5*R*)-5-(3-hydroxyphenyl)-3-((*R*)-1-phenyl-ethylamino)-1-(4-trifluoromethyl-phenyl)-pyrrolidin-2-one was supplied by the commercial supplier (PharmaSynth, Tartu, Estonia), and [^{18}F]FMPEP-d_2 syntheses were conducted as described previously (Donohue et al., 2008). For radionuclide production, fluorine-18 was produced by proton irradiation of oxygen-18. [^{18}F]FMPEP-d_2 was formulated in up to 10% ethanol in saline. The molar activity was >500 GBq/μmol at the end of each synthesis, and the molar activity at the time of the injection was calculated according to the limiting value (500 GBq/μmol) with an average of 359 GBq/μmol (standard deviation [SD] = 71 GBq/μmol) (34 batches). The radiochemical purity exceeded 95% in all syntheses.

2.2. Experimental animals

APP/PS1-21 TG mice (C57BL/6J−TgN(Thy1−APPKM670/671NL; Thy1−PS1L166P) were originally purchased from Koesler (Rottenburg, Germany) and further bred with C57BL/6Cn mice in the Central Animal Laboratory of University of Turku. APP/PS1-21 contains human transgenes for both amyloid precursor protein bearing the Swedish mutation and presenilin 1 containing L166P mutation, both under the control of the Thy1 promoter (Radde et al., 2006). Toxic Aβ42 begins to develop in the brain of this mouse model at 6 weeks of age, and peak number of the fibrillary deposits is reached at 9 months of age (Takkinen et al., 2017). WT mice from the same litter were used as control animals. All animals were housed and fed as described previously (Takkinen et al., 2017). All animal experiments were approved by the Regional State Administrative Agency for Southern Finland (ESAVI/3899/04.10.07/2013), and animal care complied with the principles of the laboratory animal care and with the guidelines of the International Council of Laboratory Animal Science. The total number of animals used in this study was 103 ($n_{TG} = 44$; $n_{WT} = 59$). The separation of experimental animals into specific study groups is illustrated in Table 1.

2.3. In vivo [^{18}F]FMPEP-d_2 PET imaging

Longitudinal data were obtained by in vivo PET imaging using APP/PS1-21 mice (n = 8, male) and WT control littermates (n = 8, male). The mice underwent PET scans at 6, 9, 12, and 15 months of

Table 1
The total number of mice used in the study

Genotype	Sex														
	APP/PS1-21							WT							
	M				F			M					F		
Age (mo)	6	9	12	15	6	9	12	2–4	6	9	12	15	6	9	12
In vivo PET imaging	8[a]	8[a]	8[a]	7[a]					8[b]	8[b]	8[b]	6[b]			
Ex vivo brain autoradiography	3	5	2	10	1	6	2		3	5	2	6	2	4	4
IHC	[c]	[c]	[c]	[c]	[c]	[c]	[c]		[c]	[c]	[c]	[c]	[c]	[c]	[c]
Western blot		3				4				3				3	
Radiometabolite analysis								15							
Pretreatment studies								4							

Key: F, female; M, male; PET, positron emission tomography; WT, wild-type.
[a] The same APP/PS1-21 mice.
[b] The same WT mice.
[c] The number of animals in immunohistochemistry (IHC) corresponds to the number in the ex vivo studies.

age using a 1.4-mm spatial resolution Inveon Multimodality PET/CT scanner (Siemens Medical Solutions, Knoxville, TN, USA).

The detailed in vivo study design is presented in Figure S1. Briefly, an intravenous bolus injection of [^{18}F]FMPEP-d_2 (2.0 MBq, SD = 0.8 MBq; injected mass 3.2 ng, SD = 1.1 ng) was delivered via a tail vein to anesthetized mice, and a 30-minute static PET list mode scan with an energy window of 350–650 keV was initiated 90 minutes after the injection.

The PET imaging data were quantified using Inveon Research Workplace Image Analysis software 4.1 (Siemens Medical Solutions) and coregistered with a 3-dimensional mouse brain magnetic resonance imaging template (Mouse Brain Template, 2005; Takkinen et al., 2017). The [^{18}F]FMPEP-d_2 binding was analyzed over the specific brain regions: the whole brain (B), frontal cortex (FC), parietotemporal cortex (PTC), HIPPO, thalamus (THALA), striatum (STR), hypothalamus (HYPO), and cerebellum (CB). The specific [^{18}F]FMPEP-d_2 binding was evaluated as ratios of regional radioactivity concentrations relative to the THALA for 90–120 minutes, and are referenced as binding ratios. The THALA was selected as a pseudo-reference region based on the low number of CB_1Rs in mouse THALA (Allen Brain Atlas), the congruent in vivo standard uptake values between TG and WT mice (Fig. 1D), and the 40% faster clearance of [^{18}F]FMPEP-d_2 from this region compared with other regions, such as PTC (Fig. 6).

2.4. Ex vivo brain autoradiography

Ex vivo [^{18}F]FMPEP-d_2 brain autoradiography studies were performed with separate 6-, 9-, 12-, and 15-month-old TG (n_{TOTAL} = 29; 20 males) and WT mice (n_{TOTAL} = 26; 16 males) (Table 1).

The detailed ex vivo study design is presented in Figure S1. Briefly, [^{18}F]FMPEP-d_2 (3.2 MBq, SD = 0.8 MBq; injected mass 3.1 ng, SD = 1.2 ng) was delivered intravenously via a tail vein to anesthetized mice, after which they were awakened. Mice were sacrificed via cardiac puncture under deep isoflurane anesthesia after a 120-minute uptake period. Transcardial perfusion was performed to remove the blood from the brain, and the brains were dissected and treated as described previously (Takkinen et al., 2017).

The digital autoradiographs were analyzed using Aida Image Analysis software (Image Analyzer v.4.22; Raytest Isotopenmeßgeräte GmbH, Straubenhardt, Germany). The [^{18}F]FMPEP-d_2 binding was analyzed over the following brain regions: FC, PTC, THALA, STR, and HYPO. In addition, HIPPO and CB were analyzed as the anterior HIPPO, posterior HIPPO (POSTH), CB gray matter, and CB white matter. Each regional background-erased photostimulated luminescence per area value was divided by the corresponding THALA value within the same subject to gain radioactivity ratios for each region of interest, which are referenced as binding ratios.

2.5. Radiometabolite analyses

The metabolite analyses were performed with 3- to 4-month-old male C57BL/6Cn mice (n_{TOTAL} = 15) at 15, 30, 60, 120, 180, and 240 minutes after [^{18}F]FMPEP-d_2 injection. Plasma and cortex samples were treated as described previously (Eriksson et al., 2015). Fractions and [^{18}F]FMPEP-d_2 standards (20 μL) were applied to Silica gel 60 HPTLC RP-18 plates (Merck 1.05914.0001), which were developed with 1% trifluoroacetic acid/acetonitrile (40:60, v/v) as the mobile phase. The proportions (%) of intact and metabolized tracer in total ^{18}F-radioactivity of the sample were calculated as described elsewhere (Snellman et al., 2012).

2.6. Blocking studies with rimonabant

The specificity of the [^{18}F]FMPEP-d_2 binding in the mouse brain was evaluated with a CB_1R-selective inverse agonist, rimonabant

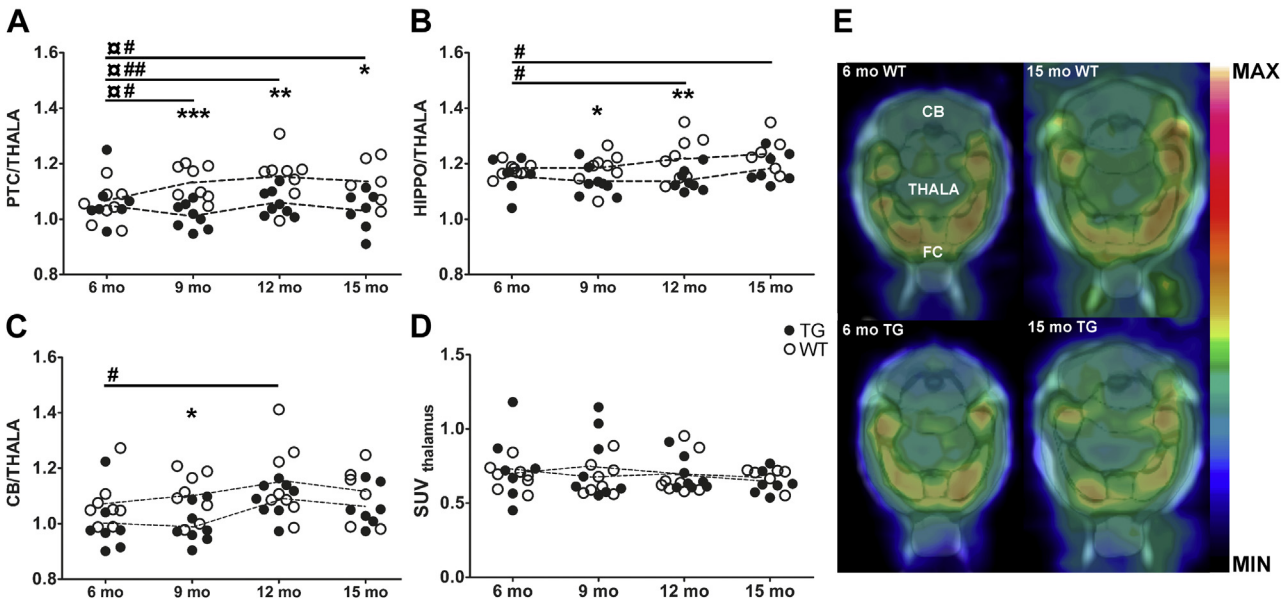

Fig. 1. Longitudinal [^{18}F]FMPEP-d_2 binding in aging APP/PS1-21 and wild-type control mice. In vivo [^{18}F]FMPEP-d_2 binding ratios relative to THALA are presented for (A) PTC, (B) HIPPO, and (C) CB of APP/PS1-21 (TG, n = 7–8; filled circles) and WT mice (n = 6–8; open circles) at 6, 9, 12, and 15 months of age. (D) THALA was used as a pseudoreference region in the in vivo analysis. (Hierarchial mixed linear model with compound symmetry covariance structure, intergroup differences between age-matched TG and WT mice $^{*}p < 0.05$, $^{**}p < 0.005$, and $^{***}p < 0.0005$; time interval differences from 6 to 9 months, 6 to 12 months, and 6 to 15 months between TG and WT mice ¤$p < 0.05$; intragroup binding differences within the same WT (and TG in CB) mice during aging #$p < 0.05$ and ##$p < 0.005$). (E) Representative axial summed [^{18}F]FMPEP-d_2 PET/CT images, coregistered with a mouse MRI-template and adjusted within the same color scale, of a TG mouse at 6 and 15 months of age (below) and a WT mouse at 6 and 15 months of age (above) demonstrate the [^{18}F]FMPEP-d_2 binding distribution differences in FC, THALA, and CB. Abbreviations: CB, cerebellum; FC, frontal cortex; HIPPO, hippocampus; mo, months; PET, positron emission tomography; PTC, parietotemporal cortex; TG, transgenic mouse; THALA, thalamus; WT, wild-type.

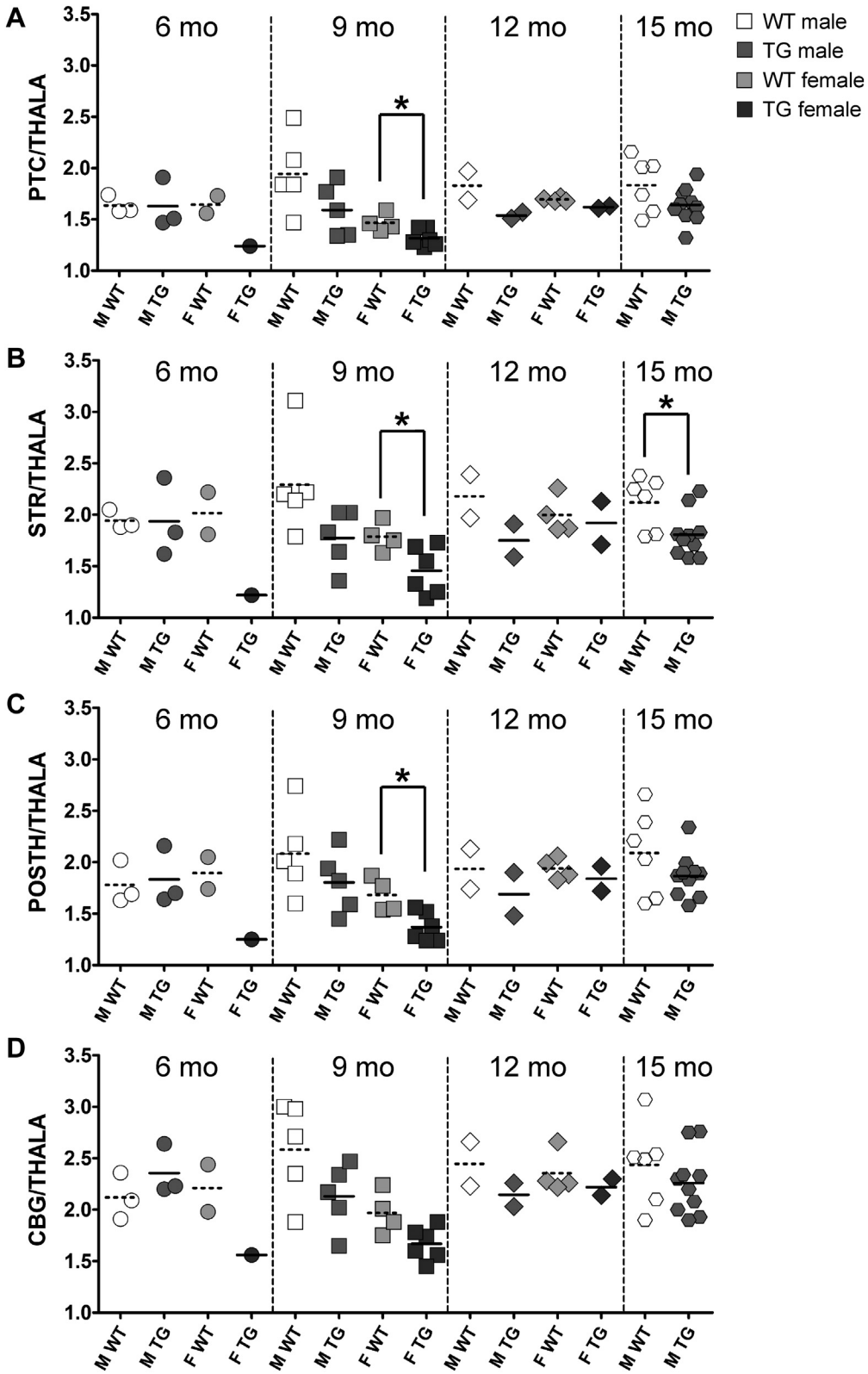

Fig. 2. Ex vivo brain [^{18}F]FMPEP-d_2 binding ratios for male and female APP/PS1-21 and WT control mice. Ex vivo [^{18}F]FMPEP-d_2 binding ratios relative to THALA are presented for (A) PTC, (B) STR, (C) posterior HIPPO (POSTH), and cerebellar gray matter (CBG) of male (M) and female (F) APP/PS1-21 (TG, $n_{TOTAL} = 29$; dark gray symbols, solid average lines) and WT mice ($n_{TOTAL} = 26$; white/light gray symbols, dashed average lines) at 6, 9, 12, and 15 months of age. (Mann–Whitney *U* test, intergroup differences between age-matched TG and WT mice $^{*}p < 0.05$). Abbreviations: HIPPO, hippocampus; PTC, parietotemporal cortex; STR, striatum; TG, transgenic mouse; THALA, thalamus; WT, wild-type.

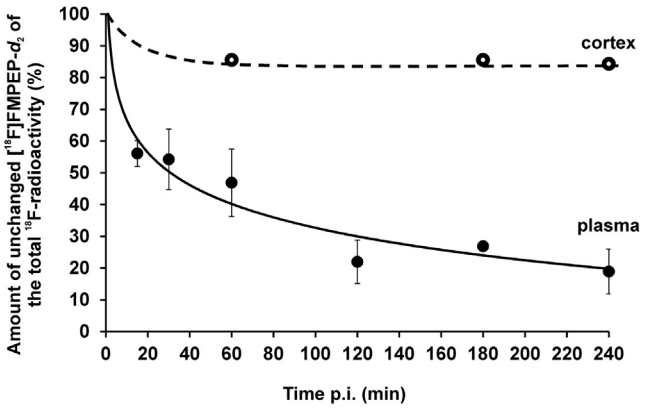

Fig. 3. Amount of the unchanged [^{18}F]FMPEP-d_2 of the total ^{18}F-radioactivity in wild-type mouse plasma and cortex. The radiometabolites were analyzed at 15, 30, 60, 120, 180, and 240 minutes (n = 1–5, mean with standard deviation) for plasma, and at 60, 180, and 240 minutes (n = 1) for cortex.

(SR141716; No. 9000484, Cayman Chemical, MI, USA) (Kenakin, 2001). Blocking studies were conducted with C57Bl/6Cn mice (n = 4; 2 months), 2 of which were pretreated with rimonabant (2 mg/kg in 20% ethanol and Kleptose β-cyclodextrin, intravenously 10 minutes before the tracer injection) and 2 with saline. The mice were anesthetized with a 2.5% isoflurane/oxygen mixture 20 minutes before pretreatment. Intravenous injection of [^{18}F]FMPEP-d_2 (3.4 MBq, SD = 0.2 MBq) and 90-minute dynamic 3-dimensional PET/CT list mode scans were started in tandem. After the scan, the mice were sacrificed and the brains treated as described previously (Takkinen et al., 2017).

2.7. Western blot

The detailed western blot study protocol is presented in Supplementary material S2. Briefly, the CB_1R abundance in the FC, PTC, HIPPO, and THALA was quantified in 9-month-old TG (n_{TOTAL} = 7; 3 males) and WT (n_{TOTAL} = 6; 3 males) mice. The brain regions were dissected and snap-frozen with liquid nitrogen. The tissue samples were homogenized on ice in a lysis buffer supplemented with a Pierce protease inhibitor tablet (#88266 Thermo Scientific). Protein concentrations were measured using a Pierce BCA protein assay kit (Thermo Scientific), and equal amounts of samples were pipetted per lane of a 10% sodium dodecyl sulfate-polyacrylamide gel and separated by electrophoresis. After the transfer, the membranes were probed with an anti-CB_1R primary antibody (1:500, Abcam Cat# ab23703, RRID:AB_447623) or a housekeeping primary anti-β-actin antibody (1:1000. Abcam Cat# ab8227, RRID:AB_2305186). A fluorescent secondary antibody (1:2000, IRDye 800CW Donkey anti-Rabbit IgG H+L, LI-COR Biosciences Cat# 925−32,211, RRID:AB_2651127) enabled the signal detection with the LI-COR Odyssey CLx Imaging System (LI-COR, Inc). The fluorescent signals were analyzed by Image Studio Software Lite v. 5.2 (LI-COR, Inc) and the signal intensities were normalized to the housekeeping protein in each membrane.

2.8. CB_1R immunohistochemistry

The localization of the CB_1Rs was visualized by staining the brain sections collected from ex vivo autoradiography. Fresh-frozen brain sections of 6- to 15-month-old mice were air-dried, postfixed with 4% paraformaldehyde, and stained with anti-CB_1R (1:500, Abcam Cat# ab23703, RRID:AB_447623). The immunohistochemical staining protocol was conducted as described previously (Takkinen et al., 2017), and sections were imaged with a 3DHISTECH Slide Scanner 250.

2.9. Statistical analysis

For the in vivo and ex vivo studies, the results are expressed as the mean group values with SD. The statistical analyses were performed using SAS System for Windows (version 9.3, SAS Institute Inc, Cary, NC, USA) and GraphPad Prism 6.0 software (GraphPad Software). For in vivo data, statistical analyses were performed using a hierarchical mixed linear model with compound symmetry covariance structure, including one within-factor (time; indicating overall mean change between baseline and other measurement), one between-factor (*genotype*; WT and TG), and the interaction term (genotype*time). Interaction was examined when the mean change during the study was different between the genotypes. The assumption of normal distribution was checked based on the studentized residuals. For ex vivo autoradiography, statistical analyses were performed with Mann−Whitney *U* test (GraphPad Prism 6.0), and for western blot with 2-way ANOVA where gender and genotype were handled as explanatory variables (SAS System). All statistical tests were performed as 2-sided with the significance level set at 0.05.

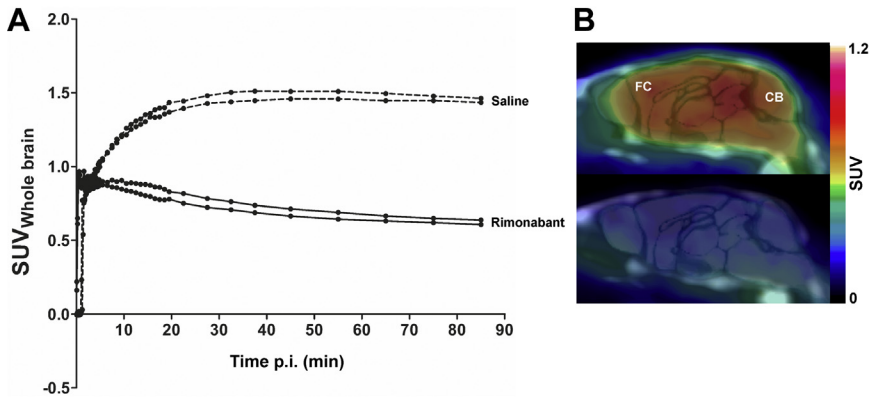

Fig. 4. Rimonabant displaced 67 % of the total [^{18}F]FMPEP-d_2 binding in the whole mouse brain. (A) The whole brain time-activity curves for dynamic 90-minute [^{18}F]FMPEP-d_2 PET/CT scan (average dose 3.4 MBq, SD 0.2 MBq) of 2 rimonabant-treated (2 mg/kg) WT mice (congruent line) and 2 saline-treated WT mice (dashed line). (B) Representative sagittal [^{18}F]FMPEP-d_2 PET/CT images, coregistered with a mouse MRI-template and adjusted within the same color scale according to [^{18}F]FMPEP-d_2 standard uptake values (SUVs), of a 4-month-old rimonabant-treated mouse (below) and saline-treated mouse (above), demonstrating the [^{18}F]FMPEP-d_2 binding difference after displacement and non-displacement. Abbreviations: CB, cerebellum; FC, frontal cortex; PET, positron emission tomography; WT, wild-type.

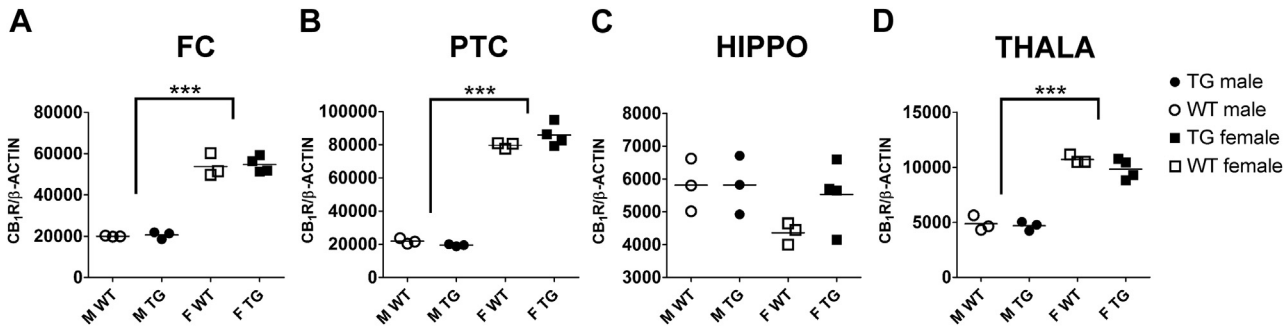

Fig. 5. The regional CB_1R expression in APP/PS1-21 and wild-type mice. The levels of CB_1R in 9-month-old male APP/PS1-21 (n = 3; filled symbols) and WT (n = 3; open symbols) mice were 3- to 4-fold lower than in age-matched female APP/PS1-21 (n = 4) and WT mice (n = 3) in (A) FC; (B) PTC, and (D) THALA. In (C) HIPPO, there was no differences between the male and female mice, or TG and WT mice. The results are displayed in normalized CB_1R/β-actin ratios, expressed as arbitrary units (2-way ANOVA, intergroup differences $^{***}p < 0.0001$). Abbreviations: CB_1R, type 1 cannabinoid receptor; FC, frontal cortex; F, female; HIPPO, hippocampus; M, male; PTC, parietotemporal cortex; TG, transgenic mouse; THALA, thalamus; WT, wild-type.

3. Results

3.1. Longitudinal PET data demonstrates lower [^{18}F]FMPEP-d_2 binding ratios for APP/PS1-21 mice compared with age-matched WT mice

During the longitudinal study, 1 TG mouse and 2 WT mice died; therefore, the number of animals was diminished at 15-month imaging age. All in vivo [^{18}F]FMPEP-d_2 binding ratios in TG and WT mice are presented in Table 2.

[^{18}F]FMPEP-d_2 THALA mean standard uptake value was 0.692 (SD = 0.154) in TG mice and 0.681 (SD = 0.103) in WT mice during the whole follow-up study (Fig. 1D). Significantly lower [^{18}F]FMPEP-d_2 HYPO/THALA ratios were measured in 6-month-old TG mice compared with age-matched WT mice. Significantly lower binding ratios were observed in the B, FC, PTC, CB, and HIPPO of 9-month-old TG mice; in the B, PTC, and HIPPO of 12-month-old TG mice; and in the FC and PTC of 15-month-old TG mice (n = 7) compared with age-matched WT mice (n = 6) in the intergroup analysis (Fig. 1).

The mean [^{18}F]FMPEP-d_2 binding ratio changes in the PTC differed significantly between TG and WT mice from 6 to 9 months of age, 6 to 12 months of age, and 6 to 15 months of age (Fig. 1A). The mean binding ratio changes in the HIPPO differed, although not significantly ($p = 0.0669$), between TG and WT mice from 6 to 9 months of age. In the other brain regions, the differences in mean binding changes did not vary throughout the longitudinal study because significant intergroup differences in binding between the TG and WT mice were already present at 6 months of age.

[^{18}F]FMPEP-d_2 binding ratios between the same aging TG mice during the longitudinal study increased significantly in CB between 6 and 12 months of age. In WT mice, significantly increased binding ratios were observed at 9 months of age in the PTC; at 12 months of age in the PTC, HIPPO, and CB; and at 15 months of age in the PTC and HIPPO, when compared with the same mice at 6 months (Fig. 1).

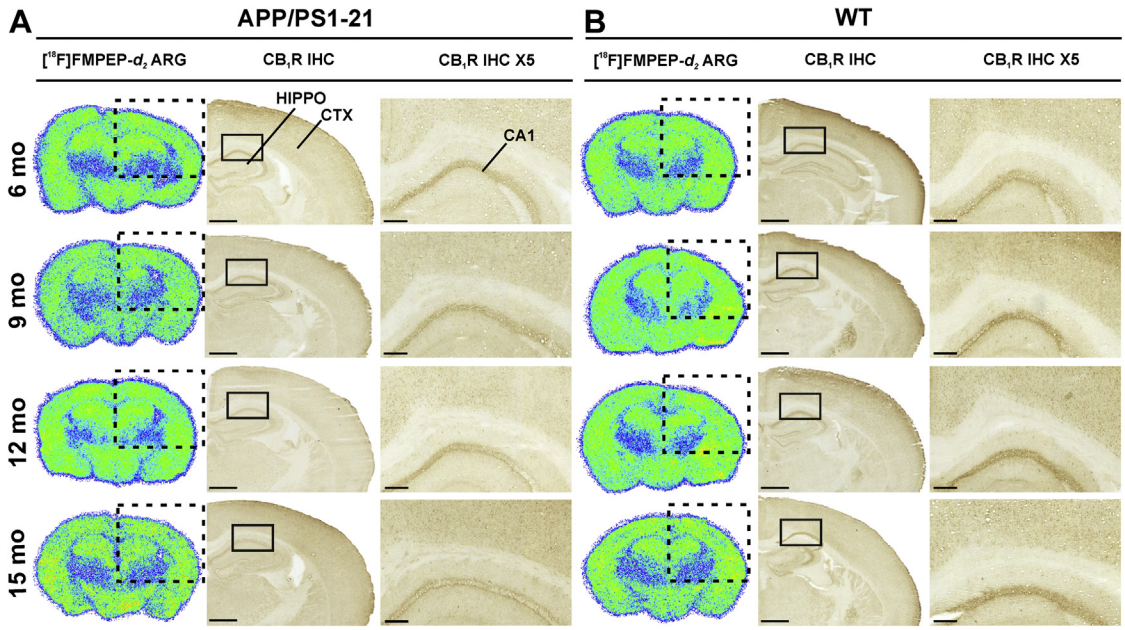

Fig. 6. CB_1R staining in APP/PS1-21 and WT mouse brain. (A) Representative ex vivo brain [^{18}F]FMPEP-d_2 autoradiographs (left column), correlative CB_1R (middle column), and 5-fold magnification of CB_1R immunohistochemical staining (right column) of 6-, 9-, 12-, and 15-month-old male APP/PS1-21 and (B) WT mouse brain sections. Scale bars in (A) and (B): 1000 μm for CB_1R brain sections; 200 μm for CB_1R IHC 5-fold magnification. Abbreviations: ARG, autoradiograph; CB_1R, type 1 cannabinoid receptor; CTX, cortex; HIPPO, hippocampus; IHC, immunohistochemistry; mo, months; WT, wild-type.

Table 2
In vivo [^{18}F]FMPEP-d_2 binding ratios relative to the thalamus in male APP/PS1-21 (n = 7–8) and wild-type (WT, n = 6–8) mice according to age and brain region

Brain region	6 mo			9 mo			12 mo			15 mo		
	TG	WT	p	TG	WT	p	TG	WT	p	TG	WT	p
Brain	1.05 ± 0.05	1.08 ± 0.05	ns	1.04 ± 0.04	1.09 ± 0.04	[a]	1.04 ± 0.02	1.10 ± 0.06	[a]	1.05 ± 0.04	1.12 ± 0.05	ns
FC	1.20 ± 0.07	1.27 ± 0.09	ns	1.16 ± 0.06	1.26 ± 0.10	[b]	1.20 ± 0.04	1.24 ± 0.08	ns	1.14 ± 0.07	1.29 ± 0.05	[b]
PTC	1.07 ± 0.08	1.05 ± 0.07	ns	1.01 ± 0.05	1.13 ± 0.06[e]	[c,d]	1.06 ± 0.05	1.15 ± 0.09[f]	[b,d]	1.03 ± 0.07	1.13 ± 0.08[e]	[a,d]
CB	0.99 ± 0.10	1.07 ± 0.09	ns	1.00 ± 0.07	1.10 ± 0.08	[a]	1.09 ± 0.06[e]	1.15 ± 0.14[e]	ns	1.06 ± 0.07	1.11 ± 0.11	ns
HIPPO	1.16 ± 0.06	1.18 ± 0.03	ns	1.14 ± 0.05	1.18 ± 0.06	[a]	1.14 ± 0.04	1.22 ± 0.08[e]	[b]	1.19 ± 0.06	1.24 ± 0.07[e]	ns
STR	1.24 ± 0.03	1.28 ± 0.09	ns	1.20 ± 0.05	1.22 ± 0.09	ns	1.20 ± 0.05	1.24 ± 0.06	ns	1.21 ± 0.08	1.28 ± 0.07	ns
HYPO	1.00 ± 0.10	1.09 ± 0.05	[a]	1.04 ± 0.06	1.01 ± 0.05	ns	1.01 ± 0.06	1.07 ± 0.11	ns	1.04 ± 0.07	1.11 ± 0.06	ns

Data are presented as the mean ± standard deviation.
Key: CB, cerebellum; FC, frontal cortex; HIPPO, hippocampus; HYPO, hypothalamus; mo, months; ns, not significant; PTC, parietotemporal cortex; STR, striatum; TG, transgenic mouse; WT, wild-type.
[a] $p < 0.05$ for intergroup differences between age-matched APP/PS1-21 and WT mice.
[b] $p < 0.005$ for intergroup differences between age-matched APP/PS1-21 and WT mice.
[c] $p < 0.0005$ for intergroup differences between age-matched APP/PS1-21 and WT mice.
[d] $p < 0.05$ for time interval differences from 6 to 9 mo, 6 to 12 mo, and 6 to 15 mo between APP/PS1-21 and WT mice.
[e] $p < 0.05$ for binding differences within the same animals during aging.
[f] $p < 0.005$ for binding differences within the same animals during aging.

3.2. Brain [^{18}F]FMPEP-d$_2$ autoradiography shows lower binding ratios in APP/PS1-21 mice compared with age-matched WT mice

All ex vivo [^{18}F]FMPEP-d_2 mean binding ratios in TG and WT mice are presented in Table S3.

In males, significantly lower binding ratios were observed in STR of 15-month-old TG mice (n = 10) compared with age-matched male WT mice (n = 6) (Fig. 2). No significant differences were observed in other brain regions, although similar trend was seen in 9-, 12-, and 15-month-old male TG mice. In 9-month-old female TG mice (n = 6), significantly decreased binding ratios were measured in the PTC, STR, and POSTH compared with age-matched female WT mice (n = 4). A similar decreasing trend was also observed in other brain regions, such as CB gray matter ($p = 0.0543$) at 9-, 12-, and 15-month-old female TG mice (Fig. 2).

3.3. Radioactive metabolites are found in plasma and brain

[^{18}F]FMPEP-d_2 metabolized slowly, producing 2 radiometabolites in plasma and 1 in the cortex. In plasma, the amount of [^{18}F]FMPEP-d_2 was approximately 56% at 15 minutes with a retention factor (Rf) of 0.3 (Fig. 3). Two polar radiometabolites in plasma had Rf values of 0.56 and 0.62. At 240 minutes, the peak proportion of unchanged tracer was approximately 19%. In the cortex, 1 polar radiometabolite was observed with an Rf value of 0.58. The ^{18}F-radioactivity in mouse cortex originated 86% from the unchanged [^{18}F]FMPEP-d_2 (Rf value 0.3) at 60 and 180 minutes, and 84% at 240 minutes after the tracer injection (Fig. 3).

3.4. Rimonabant inhibits [^{18}F]FMPEP-d$_2$ binding in mouse brain

A 2 mg/kg dose of the inverse agonist rimonabant decreased the [^{18}F]FMPEP-d_2 binding to CB_1Rs. The decay-corrected measurements using a γ-counter (Wizard^2, PerkinElmer, Finland) showed that the amounts of ^{18}F-radioactivity in the brain were 2.46 and 2.55 %ID/g in rimonabant-treated mice (n = 2), whereas in saline-treated mice, the amounts of ^{18}F-radioactivity were 7.57 and 7.44 %ID/g (n = 2). Therefore, the displacement with rimonabant was 67% in mouse brain, which was also demonstrated in in vivo concentration analyses of ^{18}F-radioactivity as a function of time (Fig. 4).

3.5. Regional CB_1R expression is unchanged between APP/PS1-21 and WT mice

Female (n = 7, 4 TG) and male (n = 6, 3 TG) mice were significantly differentiated ($p < 0.0001$) in terms of CB_1R expression in FC, PTC, and THALA at 9 months of age (Fig. 5, S4). In detail, female mice exhibited 2.7-fold (FC), 4.0-fold (PTC), and 2.2-fold (THALA) higher receptor expression compared with male mice. By contrast, no differences were seen between TG and WT mice, neither in females nor males. In HIPPO, no significant differences were seen between the genders or genotypes.

3.6. CB_1R visualization in the mouse brain

Immunohistochemical staining showed visible anti-CB_1R-immunoreactive staining loss in the CA1 pyramidal cell layer in APP/PS1-21 mice at 15 months of age, whereas the CA1 in WT mice remained intact. In the other brain regions, APP/PS1-21 mice did not demonstrate visible age-related changes in anti–CB_1R-immunoreactive CB_1Rs in the brain compared with age-matched WT mice. Representative images from the brain sections of the 6-, 9-, 12-, and 15-month-old APP/PS1-21 and WT mice are shown in Fig. 6.

4. Discussion

The comprehensive aim of this study was to investigate the role of CB_1Rs in aging APP/PS1-21 mice using longitudinal [^{18}F]FMPEP-d_2 PET imaging. Blocking studies with rimonabant were included to investigate the specificity of [^{18}F]FMPEP-d_2 binding, and PET imaging data were validated by ex vivo brain autoradiography and western blot to further analyze the characteristics of [^{18}F]FMPEP-d_2 binding in mouse brain.

Our in vivo results demonstrated that male APP/PS1-21 mice exhibited significantly lower [^{18}F]FMPEP-d_2 binding ratios in specific brain regions compared with age-matched WT mice. Furthermore, the significant mean changes in [^{18}F]FMPEP-d_2 binding from 6 months to 9, 12, and 15 months demonstrate that the CB_1R-related pathology in the PTC, and presumably the HIPPO, of male TG mice starts after 6 months, but then plateaus after 9 months. Whether the PET results originate from changes in the receptor abundance or receptor availability is unclear, however, the data collected from our western blot showed no differences between TG and WT mice in terms of CB_1R level, but the difference was significant between the sexes. Our ex vivo results are in line with the in vivo results, showing decreased [^{18}F]FMPEP-d_2 binding ratios both in male and female TG mice compared with corresponding WT mice, which is not visually detectable in the CB_1R immunohistochemical stainings (Fig. 6). Consequently, our results suggest the need to monitor CB_1R-associated pathology also in younger AD

animals in future PET studies while considering the gender differences.

Our PET imaging data might be affected by binding properties of [^{18}F]FMPEP-d_2. As an inverse agonist, the tracer favors binding to the receptors at the low-affinity conformation. Currently, there are no data available on whether [^{18}F]FMPEP-d_2 is able to cross the cell membrane and bind to intracellular CB_1Rs. Therefore, assuming that this radiotracer does not penetrate the cell, the observed changes could be attributed to the changes in the CB_1R availability in the cell membrane or changes in the receptor conformation. The amount of endogenous CB_1R ligands among TG and WT mice might also vary, which could lead to an altered number of binding sites available for [^{18}F]FMPEP-d_2. Taken together, this study demonstrates that male APP/PS1-21 mice have age- and genotype-dependent impairments in [^{18}F]FMPEP-d_2 binding to CB_1Rs, but no reductions in total receptor expression compared with age-matched WT mice.

Our results are in line with a previous study in which postmortem brain samples from AD patients exhibited impaired CB_1R function in the HIPPO and FC, followed by decreased CB_1R density at advanced stages of AD (Manuel et al., 2014). Altered CB_1R activity was not a consequence of reductions in receptor density, as seen in another report (Oddi et al., 2011) and in the present study. Preserved expression of CB_1R (Lee et al., 2010; Mulder et al., 2011), reduced CB_1R density in the HIPPO and caudate putamen (Westlake et al., 1994), or a decreased number of CB_1R-positive neurons in the FC of AD patients (Ramirez et al., 2005) has also been observed. Ramirez et al. also reported decreased CB_1R protein expression and G-protein decoupling despite preserved density (Ramirez et al., 2005). In the first CB_1R PET imaging study of AD, Ahmad et al. found no differences in CB_1R availability between AD patients and healthy subjects when using [^{18}F]MK-9470 (Ahmad et al., 2014).

In investigations with AD mouse models, the results have been as conflicting as in human studies. $APP_{SWE}/PS1_{\Delta E9}$ mice have decreased, increased or unchanged CB_1R availability depending on the age and sex of the animals, as well as the used methods (Kalifa et al., 2011; Karkkainen et al., 2012; Mulder et al., 2011). A more recent study in the same animal model reported increased cannabinoid receptor coupling in the FC and STR, but not in the HIPPO, when TG mice were compared with WT mice (Maroof et al., 2014), whereas an age-dependent reduction in CB_1R levels were reported in the neocortex of $APP_{SWE}/PS1_{\Delta E9}$ mice from 6 months of age (Aso et al., 2012). In a 3 × Tg-AD mouse model, significantly higher CB_1R mRNA expression was observed in the prefrontal cortex and dorsal HIPPO of 6- and 12-month-old male TG mice and decreased CB_1R levels in the dorsal HIPPO of 12-month-old TG mice (Bedse et al., 2014).

In our longitudinal study, the significant increase in [^{18}F]FMPEP-d_2 binding in the WT mice during aging, but not in the APP/PS1-21 mice, is in line with a previous [^{18}F]MK-9470 PET study in healthy women (Van Laere et al., 2008), in which the increase was detectable in basal ganglia, lateral temporal cortex, and limbic system. In rats, increases in the total CB_1R levels have been observed during aging in entorhinal and temporal cortex (Liu et al., 2003). By contrast, some findings do not support the present data suggesting instead that CB_1R gene expression declines in the specific brain structures during aging in both rodents and humans (Berrendero et al., 1998; Westlake et al., 1994) or remains unchanged (Belue et al., 1995; Wang et al., 2003). Region-dependent upregulation of [^{18}F]FMPEP-d_2 binding in WT mice may be related to the compensatory reaction against age-related endocannabinoid dysfunction, which has been reported in rodents (Maccarrone et al., 2001).

To date, only 1 PET study with healthy volunteers has assessed the cerebral CB_1R distribution in vivo in healthy aging in both sexes. Region-dependent and gender-related upregulation of [^{18}F]MK-9470 binding was observed with aging, and only women showed increased tracer binding during aging, whereas men showed higher tracer binding levels in early adulthood (Van Laere et al., 2008). Furthermore, several other studies have reported differences in the CB_1R brain availability between female and male rodents, suggesting either higher (Burston et al., 2010; Mateos et al., 2011) or lower (Gonzalez et al., 2005) CB_1R densities, accompanied by more efficient receptor function for female mice (Rubino and Parolaro, 2011). The divergence of findings has been explained by the presence of natural estrogens in females, which has been shown to regulate CB_1R expression in the brain (Riebe et al., 2010).

One limitation of our study was the small sample size in the ex vivo and western blot experiments. Also the primary pathology of APP/PS1-21 mouse model, β-amyloidosis, was not examined. This could have improved the conclusions of the [^{18}F]FMPEP-d_2 binding in relation to the β-amyloid pathology, although the temporal course of amyloid deposition of this model has been reported previously with 6-, 9-, 12-, and 15-month-old animals (Takkinen et al., 2017). In the western blot, the CB_1R expression difference between female and male mice was congruent between groups and as great as 3- to 4-fold in the FC, PTC, and THALA (Fig. 5); therefore, we do not believe that a larger group size would have affected the western blot results. However, additional age groups would have provided specific information about the etiology behind the differences between the sexes and genotypes. The ex vivo results supported the longitudinal imaging data only for STR, presumably due to the small sample size of the groups. The statistical power of the longitudinal imaging examination, thus, is strong, especially when monitoring repeatedly the same animals per research group. Therefore, we believe that no underachievement was present in this study because of the longitudinal study protocol for [^{18}F]FMPEP-d_2.

Furthermore, 1 radioactive metabolite of [^{18}F]FMPEP-d_2 was found in the brain; however, the brain metabolite was not identified or characterized so it may have binding selectivity for CB_1Rs or distribute nonspecifically across all brain regions. This metabolite probably has peripheral origin because the same metabolite was found in plasma.

5. Conclusions

This study is the first longitudinal imaging study in which [^{18}F]FMPEP-d_2 was used to monitor CB_1R changes in the AD mice. Our study demonstrated age- and genotype-dependent alterations in [^{18}F]FMPEP-d_2 binding to CB_1Rs in male TG mice and unchanged CB_1R total expression at the same age. This study presents encouraging evidence of the applicability of this tracer, especially for monitoring availability of CB_1Rs in neurodegenerative diseases. However, additional PET studies are needed to evaluate the binding differences between sexes and to confirm the proposed potential of [^{18}F]FMPEP-d_2 as a PET tracer for imaging CB_1Rs in AD. Enhancing knowledge about pharmacological approaches for targeting cannabinoid receptors with suitable imaging methods is a promising strategy to prevent or delay AD.

Disclosure statement

The authors have no actual or potential conflicts of interest.

Acknowledgements

The authors thank the staff at the Accelerator Laboratory and the Radiopharmaceutical Chemistry Laboratory for radionuclide production and tracer analyses and also thank Aake Honkaniemi, Elisa Riuttala, and Marko Vehmanen in the Medicity Research Laboratory for assistance with the animal experiments.

This work was supported by the Doctoral Programme in Clinical Research at the University of Turku, the European Community's 7th framework programme (FP7/2007–2013) under grant agreement no. HEALTH-F2-2011–278850 (INMiND), the Alfred Kordelin Foundation, the Instrumentarium Science Foundation, state research funding from the Hospital District of Southern Finland, the Finnish Brain Foundation sr, and by a grant from the Academy of Finland (no. 266891).

Appendix A. Supplementary data

Supplementary data associated with this article can be found, in the online version, at https://doi.org/10.1016/j.neurobiolaging.2018.05.013.

References

Ahmad, R., Goffin, K., Van den Stock, J., De Winter, F.L., Cleeren, E., Bormans, G., Tournoy, J., Persoons, P., Van Laere, K., Vandenbulcke, M., 2014. In vivo type 1 cannabinoid receptor availability in Alzheimer's disease. Eur. Neuropsychopharmacol. 24, 242–250.

Allen Brain Atlas. Available at. http://www.brain-map.org/. Search term: CB1R. Accessed March 6, 2018.

Aso, E., Palomer, E., Juves, S., Maldonado, R., Munoz, F.J., Ferrer, I., 2012. CB1 agonist ACEA protects neurons and reduces the cognitive impairment of AbetaPP/PS1 mice. J. Alzheimers Dis. 30, 439–459.

Ball, M.J., 1976. Neurofibrillary tangles in the dementia of "normal pressure" hydrocephalus. Can. J. Neurol. Sci. 3, 227–235.

Bedse, G., Romano, A., Cianci, S., Lavecchia, A.M., Lorenzo, P., Elphick, M.R., Laferla, F.M., Vendemiale, G., Grillo, C., Altieri, F., Cassano, T., Gaetani, S., 2014. Altered expression of the CB1 cannabinoid receptor in the triple transgenic mouse model of Alzheimer's disease. J. Alzheimers Dis. 40, 701–712.

Belue, R.C., Howlett, A.C., Westlake, T.M., Hutchings, D.E., 1995. The ontogeny of cannabinoid receptors in the brain of postnatal and aging rats. Neurotoxicol. Teratol. 17, 25–30.

Benito, C., Nunez, E., Tolon, R.M., Carrier, E.J., Rabano, A., Hillard, C.J., Romero, J., 2003. Cannabinoid CB2 receptors and fatty acid amide hydrolase are selectively overexpressed in neuritic plaque-associated glia in Alzheimer's disease brains. J. Neurosci. 23, 11136–11141.

Berrendero, F., Romero, J., Garcia-Gil, L., Suarez, I., De la Cruz, P., Ramos, J.A., Fernandez-Ruiz, J.J., 1998. Changes in cannabinoid receptor binding and mRNA levels in several brain regions of aged rats. Biochim. Biophys. Acta 1407, 205–214.

Burns, H.D., Van Laere, K., Sanabria-Bohorquez, S., Hamill, T.G., Bormans, G., Eng, W.S., Gibson, R., Ryan, C., Connolly, B., Patel, S., Krause, S., Vanko, A., Van Hecken, A., Dupont, P., De Lepeleire, I., Rothenberg, P., Stoch, S.A., Cote, J., Hagmann, W.K., Jewell, J.P., Lin, L.S., Liu, P., Goulet, M.T., Gottesdiener, K., Wagner, J.A., de Hoon, J., Mortelmans, L., Fong, T.M., Hargreaves, R.J., 2007. [18F] MK-9470, a positron emission tomography (PET) tracer for in vivo human PET brain imaging of the cannabinoid-1 receptor. Proc. Natl. Acad. Sci. U S A 104, 9800–9805.

Burston, J.J., Wiley, J.L., Craig, A.A., Selley, D.E., Sim-Selley, L.J., 2010. Regional enhancement of cannabinoid CB_1 receptor desensitization in female adolescent rats following repeated Delta-tetrahydrocannabinol exposure. Br. J. Pharmacol. 161, 103–112.

Charalambous, A., Marciniak, G., Shiue, C.Y., Dewey, S.L., Schlyer, D.J., Wolf, A.P., Makriyannis, A., 1991. PET studies in the primate brain and biodistribution in mice using (-)-5'-18F-delta 8-THC. Pharmacol. Biochem. Behav. 40, 503–507.

Donohue, S.R., Krushinski, J.H., Pike, V.W., Chernet, E., Phebus, L., Chesterfield, A.K., Felder, C.C., Halldin, C., Schaus, J.M., 2008. Synthesis, ex vivo evaluation, and radiolabeling of potent 1,5-diphenylpyrrolidin-2-one cannabinoid subtype-1 receptor ligands as candidates for in vivo imaging. J. Med. Chem. 51, 5833–5842.

Eriksson, O., Mikkola, K., Espes, D., Tuominen, L., Virtanen, K., Forsback, S., Haaparanta-Solin, M., Hietala, J., Solin, O., Nuutila, P., 2015. The cannabinoid receptor-1 is an imaging biomarker of brown adipose tissue. J. Nucl. Med. 56, 1937–1941.

Fagan, S.G.A.C., Campbell, V.A., 2015. Endocannabinoids and Alzheimer's disease. In: Fattore, L. (Ed.), Cannabinoids in Neurologic and Mental Disease, first ed. Academic Press, Oxford, pp. 15–27.

Glenner, G.G., Wong, C.W., Quaranta, V., Eanes, E.D., 1984. The amyloid deposits in Alzheimer's disease: their nature and pathogenesis. Appl. Pathol. 2, 357–369.

Gonzalez, S., Mena, M.A., Lastres-Becker, I., Serrano, A., de Yebenes, J.G., Ramos, J.A., Fernandez-Ruiz, J., 2005. Cannabinoid CB1 receptors in the basal ganglia and motor response to activation or blockade of these receptors in parkin-null mice. Brain Res. 1046, 195–206.

Hirvonen, J., Zanotti-Fregonara, P., Umhau, J.C., George, D.T., Rallis-Frutos, D., Lyoo, C.H., Li, C.T., Hines, C.S., Sun, H., Terry, G.E., Morse, C., Zoghbi, S.S., Pike, V.W., Innis, R.B., Heilig, M., 2013. Reduced cannabinoid CB1 receptor binding in alcohol dependence measured with positron emission tomography. Mol. Psychiatry 18, 916–921.

Horti, A.G., Fan, H., Kuwabara, H., Hilton, J., Ravert, H.T., Holt, D.P., Alexander, M., Kumar, A., Rahmim, A., Scheffel, U., Wong, D.F., Dannals, R.F., 2006. [^{11}C] JHU75528: a radiotracer for PET imaging of CB1 cannabinoid receptors. J. Nucl. Med. 47, 1689–1696.

Kalifa, S., Polston, E.K., Allard, J.S., Manaye, K.F., 2011. Distribution patterns of cannabinoid CB1 receptors in the hippocampus of APPswe/PS1DeltaE9 double transgenic mice. Brain Res. 1376, 94–100.

Karkkainen, E., Tanila, H., Laitinen, J.T., 2012. Functional autoradiography shows unaltered cannabinoid CB1 receptor signalling in hippocampus and cortex of APP/PS1 transgenic mice. CNS Neurol. Disord. Drug Targets 11, 1038–1044.

Karl, T., Cheng, D., Garner, B., Arnold, J.C., 2012. The therapeutic potential of the endocannabinoid system for Alzheimer's disease. Expert Opin. Ther. Targets 16, 407–420.

Kenakin, T., 2001. Inverse, protean, and ligand-selective agonism: matters of receptor conformation. FASEB J. 15, 598–611.

Lee, J.H., Agacinski, G., Williams, J.H., Wilcock, G.K., Esiri, M.M., Francis, P.T., Wong, P.T., Chen, C.P., Lai, M.K., 2010. Intact cannabinoid CB1 receptors in the Alzheimer's disease cortex. Neurochem. Int. 57, 985–989.

Li, Z., Gifford, A., Liu, Q., Thotapally, R., Ding, Y.S., Makriyannis, A., Gatley, S.J., 2005. Candidate PET radioligands for cannabinoid CB1 receptors: [^{18}F]AM5144 and related pyrazole compounds. Nucl. Med. Biol. 32, 361–366.

Liu, P., Bilkey, D.K., Darlington, C.L., Smith, P.F., 2003. Cannabinoid CB1 receptor protein expression in the rat hippocampus and entorhinal, perirhinal, postrhinal and temporal cortices: regional variations and age-related changes. Brain Res. 979, 235–239.

Mouse MRI brain template, 2005. MRM nat mouse brain database. McKnight Brain Institute. Available at. http://brainatlas.mbi.ufl.edu/Database/. Accessed May 17 2013.

Maccarrone, M., Attina, M., Bari, M., Cartoni, A., Ledent, C., Finazzi-Agro, A., 2001. Anandamide degradation and N-acylethanolamines level in wild-type and CB1 cannabinoid receptor knockout mice of different ages. J. Neurochem. 78, 339–348.

Manuel, I., Gonzalez de San Roman, E., Giralt, M.T., Ferrer, I., Rodriguez-Puertas, R., 2014. Type-1 cannabinoid receptor activity during Alzheimer's disease progression. J. Alzheimers Dis. 42, 761–766.

Manuel, I., Lombardero, L., LaFerla, F.M., Giménez-Llort, L., Rodríguez-Puertas, R., 2016. Activity of muscarinic, galanin and cannabinoid receptors in the prodromal and advanced stages in the triple transgenic mice model of Alzheimer's disease. Neuroscience 329, 284–293.

Maroof, N., Ravipati, S., Pardon, M.C., Barrett, D.A., Kendall, D.A., 2014. Reductions in endocannabinoid levels and enhanced coupling of cannabinoid receptors in the striatum are accompanied by cognitive impairments in the AbetaPPswe/PS1DeltaE9 mouse model of Alzheimer's disease. J. Alzheimers Dis. 42, 227–245.

Mateos, B., Borcel, E., Loriga, R., Luesu, W., Bini, V., Llorente, R., Castelli, M.P., Viveros, M.P., 2011. Adolescent exposure to nicotine and/or the cannabinoid agonist CP 55,940 induces gender-dependent long-lasting memory impairments and changes in brain nicotinic and CB1 cannabinoid receptors. J. Psychopharmacol. 25, 1676–1690.

Mathews, W.B., Scheffel, U., Finley, P., Ravert, H.T., Frank, R.A., Rinaldi-Carmona, M., Barth, F., Dannals, R.F., 2000. Biodistribution of [^{18}F]SR144385 and [^{18}F] SR147963: selective radioligands for positron emission tomographic studies of brain cannabinoid receptors. Nucl. Med. Biol. 27, 757–762.

Mulder, J., Zilberter, M., Pasquare, S.J., Alpar, A., Schulte, G., Ferreira, S.G., Kofalvi, A., Martin-Moreno, A.M., Keimpema, E., Tanila, H., Watanabe, M., Mackie, K., Hortobagyi, T., de Ceballos, M.L., Harkany, T., 2011. Molecular reorganization of endocannabinoid signalling in Alzheimer's disease. Brain 134 (Pt 4), 1041–1060.

Oddi, S., Dainese, E., Fezza, F., Lanuti, M., Barcaroli, D., De Laurenzi, V., Centonze, D., Maccarrone, M., 2011. Functional characterization of putative cholesterol binding sequence (CRAC) in human type-1 cannabinoid receptor. J. Neurochem. 116, 858–865.

Pazos, M.R., Nunez, E., Benito, C., Tolon, R.M., Romero, J., 2004. Role of the endocannabinoid system in Alzheimer's disease: new perspectives. Life Sci. 75, 1907–1915.

Radde, R., Bolmont, T., Kaeser, S.A., Coomaraswamy, J., Lindau, D., Stoltze, L., Calhoun, M.E., Jaggi, F., Wolburg, H., Gengler, S., Haass, C., Ghetti, B., Czech, C., Holscher, C., Mathews, P.M., Jucker, M., 2006. Abeta42-driven cerebral amyloidosis in transgenic mice reveals early and robust pathology. EMBO Rep. 7, 940–946.

Ramirez, B.G., Blazquez, C., Gomez del Pulgar, T., Guzman, M., de Ceballos, M.L., 2005. Prevention of Alzheimer's disease pathology by cannabinoids: neuroprotection mediated by blockade of microglial activation. J. Neurosci. 25, 1904–1913.

Riebe, C.J., Hill, M.N., Lee, T.T., Hillard, C.J., Gorzalka, B.B., 2010. Estrogenic regulation of limbic cannabinoid receptor binding. Psychoneuroendocrinology 35, 1265–1269.

Rubino, T., Parolaro, D., 2011. Sexually dimorphic effects of cannabinoid compounds on emotion and cognition. Front. Behav. Neurosci. 5, 64.

Snellman, A., Rokka, J., López-Picón, F.R., Eskola, O., Wilson, I., Farrar, G., Scheinin, M., Solin, O., Rinne, J.O., Haaparanta-Solin, M., 2012. Pharmacokinetics of [^{18}F]flutemetamol in wild-type rodents and its binding to beta amyloid deposits in a mouse model of Alzheimer's disease. Eur. J. Nucl. Med. Mol. Imaging 39, 1784–1795.

Stumm, C., Hiebel, C., Hanstein, R., Purrio, M., Nagel, H., Conrad, A., Lutz, B., Behl, C., Clement, A.B., 2013. Cannabinoid receptor 1 deficiency in a mouse model of Alzheimer's disease leads to enhanced cognitive impairment despite of a reduction in amyloid deposition. Neurobiol. Aging 34, 2574–2584.

Takkinen, J.S., López-Picón, F.R., Al Majidi, R., Eskola, O., Krzyczmonik, A., Keller, T., Loyttyniemi, E., Solin, O., Rinne, J.O., Haaparanta-Solin, M., 2017. Brain energy metabolism and neuroinflammation in ageing APP/PS1-21 mice using longitudinal [^{18}F]FDG and [^{18}F]DPA-714 PET imaging. J. Cereb. Blood Flow Metab. 37, 2870–2882.

Terry, G., 2009. In vivo imaging of the cannabinoid CB1 receptor using positron emission tomography. Karolinska Institutet, Stockholm, Sweden.

Tsujikawa, T., Zoghbi, S.S., Hong, J., Donohue, S.R., Jenko, K.J., Gladding, R.L., Halldin, C., Pike, V.W., Innis, R.B., Fujita, M., 2014. In vitro and in vivo evaluation of [^{11}C]SD5024, a novel PET radioligand for human brain imaging of cannabinoid CB_1 receptors. Neuroimage 84, 733–741.

Van Laere, K., Goffin, K., Casteels, C., Dupont, P., Mortelmans, L., de Hoon, J., Bormans, G., 2008. Gender-dependent increases with healthy aging of the human cerebral cannabinoid-type 1 receptor binding using [^{18}F]MK-9470 PET. Neuroimage 39, 1533–1541.

Wang, L., Liu, J., Harvey-White, J., Zimmer, A., Kunos, G., 2003. Endocannabinoid signaling via cannabinoid receptor 1 is involved in ethanol preference and its age-dependent decline in mice. Proc. Natl. Acad. Sci. U S A 100, 1393–1398.

Westlake, T.M., Howlett, A.C., Bonner, T.I., Matsuda, L.A., Herkenham, M., 1994. Cannabinoid receptor binding and messenger RNA expression in human brain: an in vitro receptor autoradiography and in situ hybridization histochemistry study of normal aged and Alzheimer's brains. Neuroscience 63, 637–652.